Particles I

Access the latest eBook →

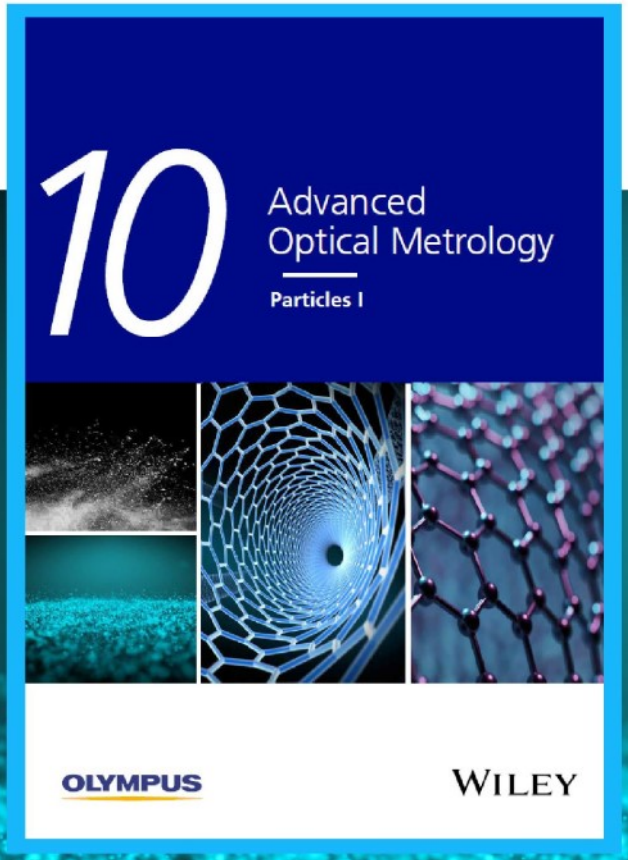

Particles: Unique Properties, Uncountable Applications

Read the latest eBook and better your knowledge with highlights from the recent studies on the design and characterization of micro- and nanoparticles for different application areas.

Access Now

This eBook is sponsored by

OLYMPUS

WILEY

ADVANCED FUNCTIONAL MATERIALS
www.afm-journal.de

Wet-Adhesive Elastomer for Liquid Metal-Based Conformal Epidermal Electronics

Jinhao Cheng, Jin Shang, Shuaijian Yang, Jiabin Dou, Xinghua Shi, and Xingyu Jiang**

Wearable electronics are increasingly used in health monitoring and treatment in different conditions. However, few devices can adhere conformally to the skin after sports and showers (sweating, deformation, friction). Here, a facile method is presented by providing a metal-polymer conductor (MPC) made with polyethylene glycol (PEG) blended polydimethylsiloxane (PDMS) based adhesive (PPA) that encapsulates gallium-based liquid metal alloy circuits as epidermal electronics. Adding PEG into PDMS prepolymer can result in a softer and wet-adhesive elastomer that can bear larger deformation than PDMS itself. The soft and adhesive electronics can adhere to the skin conformally for more than 2 d. It has been demonstrated that these electronics can meet the needs of motion detection, electrophysiological signal detection and skin wound healing during a 48 h wearing with sports and shower. It is expected that the wet-adhesive electronic with excellent biosafety can be widely used and solve existing problems in medical adhesives and human–machine interfaces.

1. Introduction

With the rapid development of material science and electrical engineering, flexible electronics have garnered significant attention and become useful in daily life.[1–4] An indispensable application of flexible electronics is real-time healthcare monitoring and on-demand treatment.[5–8] Compared to traditional rigid healthcare devices, flexible and wearable electronics can be thinner, softer and more flexible,[9–11] thus can improve the wearing experience, signal detection,[12–15] and efficiency in treatment.[16–18] A problem need to be solved is how to integrate the device firmly with the body and realize a conformal contact for a long time, particularly in situations that are challenging for electronics but regularly occur in daily life, e.g., sports and shower (sweating, deformation, friction). Different strategies like using microneedle array,[19,20] biomimetic structure design,[21,22] adhesive hydrogel,[23–26] and other polymeric adhesives[27–29] have been used to solve the problem. However, problems like skin damage caused by invasive microneedle, water loss of hydrogel, modulus mismatching with skin and bad breathability of adhesive may cause invalidation of device or allergy of skin after short time of wearing. Also, the complex synthesis or fabrication method and high costs make it impossible for large-scale fabrication and commercial use.

Polydimethylsiloxane (PDMS) is a kind of elastomer with excellent biocompatibility and permeability, making it a good choice for epidermal electronics.[30,31] However, cross-linked PDMS itself is neither adhesive nor soft enough for conformal integration with skin. There are already attempts of making PDMS a softer and more sticky elastomer by decreasing its degree of cross-linking by solvent thermal curing,[32] adding chemical reagents[33–35] or decreasing the amount of cross-linking agent.[36] While extreme conditions needed for reaction or the addition of unsafe chemical reagents strongly limit the potential applications in medical scenarios.

Here, we present a simple and safe method for tuning PDMS-based metal-polymer conductor (MPC) into wet-adhesive electronics with lower modulus and higher elongation. The soft and wet-adhesive electronics can conformally adhere to skin with sweat, water flushing and continuous deformation. Based on these characteristics, the electronics can be used for motion detection, electrophysiology and skin wound healing (**Figure 1**a). PDMS elastomer like Sylgard 184 contains two-part, double-ended vinyl polydimethylsiloxane and hydrosiloxane. In the curing process, the vinyl group can react with the hydrosiloxane with the catalysis of platinum catalyst and form a highly cross-linked network. But when a certain amount of PEG oligomer is added into the PDMS precursor and mixed well, the oligomer can adhere and surround the platinum catalyst to decrease the contact between the precursor and Pt catalyst. Previous research indicated that the PEG is able to form a complex with Pt (IV), and that may be the reason why adding PEG significantly slows the hydrosilylation,[37] decreases the degree of cross-linking and results in a lowly cross-linked network (Figure 1b). The PEG-PDMS adhesive (PPA) composed of

J. Cheng, J. Shang, S. Yang, J. Dou, X. Jiang
Shenzhen Key Laboratory of Smart Healthcare Engineering
Department of Biomedical Engineering
Southern University of Science and Technology
No. 1088, Xueyuan Rd., Xili, Nanshan District, Shenzhen, Guangdong 518055, P. R. China
E-mail: jiang@sustech.edu.cn
J. Cheng, J. Shang, J. Dou, X. Shi, X. Jiang
CAS Center for Excellence in Nanoscience
National Center for Nanoscience and Technology
Beijing 100190, P. R. China
E-mail: shixh@nanoctr.cn
J. Cheng, J. Shang, J. Dou, X. Shi, X. Jiang
University of Chinese Academy of Sciences
Beijing 100049, P. R. China
The ORCID identification number(s) for the author(s) of this article can be found under https://doi.org/10.1002/adfm.202200444.

DOI: 10.1002/adfm.202200444

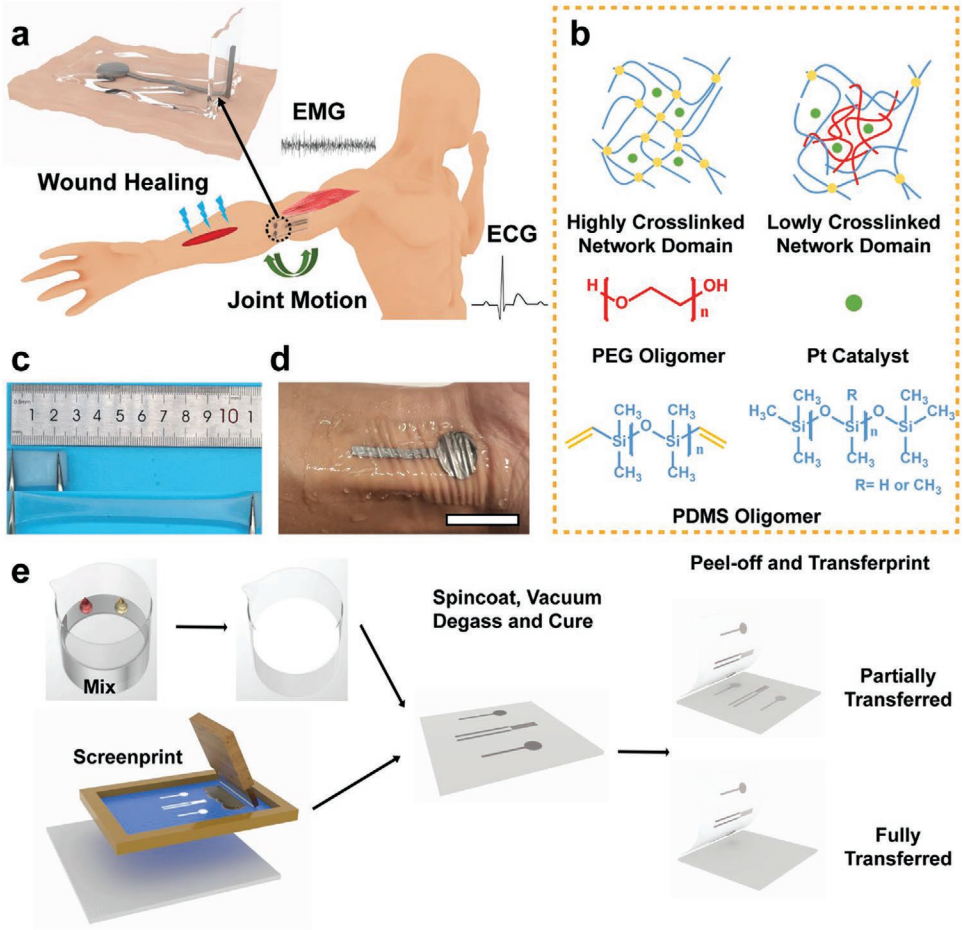

Figure 1. Schematic illustration of PPA and PPA-MPC electronics. a) Conceptual illustration of the PPA. b) The material scheme shows the highly cross-linked network domain in normally cured PDMS and lowly cross-linked network domain in PPA. c) Digital image of the elongation of the PPA under stretching (thickness of sample: 500 µm). d) Digital image of the PPA attached to the skin of the wrist with deformation after sports and water flushing (scale bar: 2 cm, thickness of sample: 150 µm). e) Fabrication process of the PPA-MPC electronics. Red drop and yellow drop represent PEG oligomer and PDMS curing agent respectively (colored just for distinguishing).

loosely cross-linked network exhibits excellent softness, stickiness and stretchability (Figure 1c,d). The soft and thin PPA is permeable to moisture and can conformally adhere to the skin, so it can maintain strong adhesion with the skin for a longer time even with sweat and large deformation. PPA also shows excellent biosafety and skin compatibility.

Gallium-based liquid metal has shown great biocompatibility, conductivity and fluidity, making it a great choice for constructing complex electronics and delivery systems.[38–42] The conception of using liquid metal based flexible electronics in health monitoring[43–45] and treatment[46–48] in different fields has been raised before. Our group has applied various MPC electronics for diagnosis and therapy in vitro and in vivo.[14–18,26,29,45] Here, we choose the liquid alloy as the conductive part of the electronics for it allows larger deformation and conformal contact with the skin. The straightforward spin-coating fabrication method can make sure the PPA encapsulates liquid metal better and increase the long-term stability of the electronics (Figure 1e). We demonstrated that the PPA-MPC electronics could adhere on skin conformally, maintain low noise and make accurate detection of the joint motion and electrophysiology signal during a period of 2 d with sports and shower. An animal model of skin wound was also performed with PPA-MPC for the demonstration of its potential in accelerating skin wound recovery.

2. Results and Discussion

2.1. Preparation and Characterization of PPA

As the adhesive substrate for electronic, the preparation of PPA is straightforward. We added the PDMS prepolymer and curing agent by the ratio of 10:1 and a certain amount of polyethylene glycol into a container and mixed well. After that, the precursor was spin-coated on a substrate, degassed under vacuum for one hour and cured at 80 °C for 1 h. (Hereafter, PDMS or PDMS-based elastomer refers to Sylgard 184 unless otherwise specified.)

To prevent the defect caused by the uncontrolled evaporation of the solvent and improve the mechanical performance of the elastomer,[49] we selected the PEG oligomers that are in the

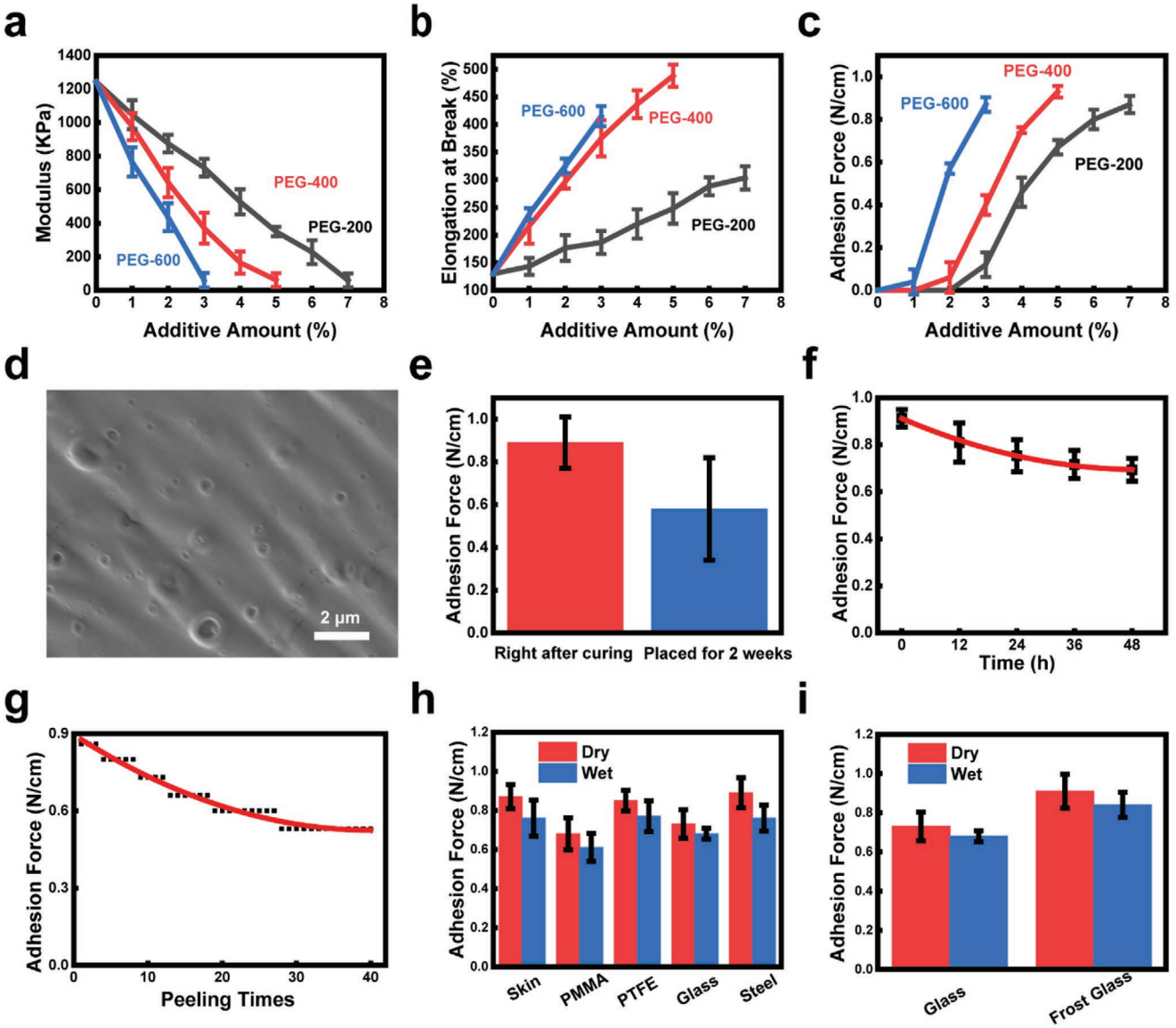

Figure 2. Mechanical and adhesion properties of PPA. a) Change of modulus with different kinds and amount of PEG oligomers added. b) Change of elongation at break with different kinds and amounts of PEG oligomers added. c) Change of adhesion force on forearm skin with different kinds and amounts of PEG oligomers added. d) SEM image of the surface morphology of PPA. e) Change of adhesion force for just-cured samples and samples placed for 2 weeks. f) Change of peeling force on forearm skin after different times of wearing. g) Change of peeling force on forearm skin after continuous peeling. h) Adhesion force on various substrates under wet and dry conditions. i) Adhesion force on common glass and frost glass under wet and dry conditions.

liquid state at room temperature with the molecular weight of 200, 400 and 600. We found that the mechanical and adhesion properties of PPA could be easily tuned by changing the type or the amount of PEG oligomer added. We tested the maximum ratio of different PEG oligomers and found the critical ratio for PEG-200, PEG-400 and PEG-600 in PPA fabricated via our method are 7.2%, 4.7%, and 3.1%. We investigated the modulus (**Figure 2**a), elongation at break (Figure 2b) and adhesion force on the forearm skin (Figure 2c) of adhesives with different ratios of PEG oligomer added. When the relative amounts were the same, the group of PEG-600 showed a lower modulus, higher elongation at break and higher adhesion force. And when added with the maximum amount, the modulus and adhesion force of the elastomer seemed to be the same, about 30 kPa and 0.9 N cm^{-1}, respectively. But things were different for elongation at break; the group of PEG-400 showed the best elongation, and the group of PEG-200 showed the worst with the maximum adding ratio. From a view of polymer chain interaction, we speculated that the oligomers in the PDMS network not only wrapped the Pt catalyst but also entangled with the silane network thus slightly increasing the elongation when stretched. The transparency of PPA with different PEG ratios and thickness was characterized using digital image and UV-Vis spectrum. We found the transparency sharply decreased as the thickness of PPA and relative amount of PEG increased (Figure S1, Supporting Information). From the upon test, we

considered the best formula for use was to add 4.7% weight of PEG-400 oligomer in PDMS mixture to obtain an elastomer with better adhesion and mechanical properties. Hereafter, PPA refers to PDMS elastomer with a 4.7% weight of PEG-400 oligomer added unless otherwise specified.

Using the as-fabricated PPA, we performed the swelling test and sol extraction test and found that with the addition of PEG, the ratio of sol part in the PPA was much higher than that of the normally cured PDMS, indicating a much lower density of cross-linking point (Text S1, Supporting Information). In the rheology test, the frequency dependence of G´ and G´´ for PPA was more significant than that of the normally cured PDMS which supported the result of the swelling test and sol extraction test (Figure S2, Supporting Information).

Scanning electron microscope (SEM) was used to characterize the surface morphology of the PPA. We found that the upper side of the adhesive is full of wrinkles (Figure 2d). The atomic force microscopy (AFM) was used to characterize the surface roughness of the adhesive, and the depth of the wrinkle was about 40 nm (Figure S3, Supporting Information). The wrinkles were formed due to the polymer chain entanglement and delayed curing process.[50] Previous research has shown that the wrinkles on the surface can increase adhesion force since the wrinkles help the adhesive wetting the surface better and thus increasing the van der Waals forces between the interfaces.[51] We tested the water contact angle (WCA) of PDMS and PPA. The PPA showed a large WCA at initial contact with water and becomes smaller 10 min later. We speculated that the phenomenon is due to the hydrophobic wrinkles and water-absorbing ability of hydrophilic PEG oligomer (Figure S4, Supporting Information).

The on-skin adhesion test was carried out by attaching the PPA to the forearm skin and peeling it off. The retention efficiency for the adhesion properties of PPA at room temperature were tested by attaching the just-cured PPA and PPA placed for 14 d to the forearm skin separately and testing the peeling force for each group. The peeling force of the just-cured PPA was 0.87 N/cm and that of the PPA cured two-weeks ago was 0.54 N cm^{-1} (Figure 2e). The difference in peeling force is mainly due to the slowly catalyzed hydrosilylation reaction by unwrapped Pt catalyst. But the adhesion force for PPA after a two-week-placing could still make sure that it adhered firmly on the forearm skin. We tested the peeling force of PPA with different attaching times. The adhesion force slightly decreased from 0.9 to 0.63 N cm^{-1} after 48 h (Figure 2f). At last we did the cycling adhering-peeling test. After 40 times of adhering and peeling, the adhesion force was still higher than 0.5 N cm^{-1}, which means the PPA could still be used as an epidermal adhesive after continuous peeling (Figure 2g). The residue test of cycling peeling was carried out, and there was no residue after 20 times of peeling (Figure S5, Supporting Information). The on-skin performance of PPA showed its potential in longtime health monitoring.

We tested the adhesion force of the PPA for different substrates under dry and wet conditions, and there was no significant decrease in adhesion force for wet condition compared to dry condition, indicating the excellent wet-adhesion properties of PPA (Figure 2h). We also found that the adhesion force for frost glass was higher than that of slippy glass, so we considered that the soft and wrinkled surface structure of the adhesive might contribute to improved wetting and increased contact area, leading to the increase of adhesion force between the interface (Figure 2i).

2.2. Biocompatibility and Longtime Properties of PPA

Biocompatibility is of great importance in longtime health monitoring. So we tested the cell viability and skin compatibility of the PPA. Bright-field (BF) and fluorescent live/dead staining images showed a regular cell morphology and few dead cells in both groups (**Figure 3**a), indicating the PPA is not toxic to the cell. The cell viability tests were also performed on liquid metal circuits, showing that the cell compatibility for liquid metal is good as well. (Figure S6, Supporting Information)

But how to prevent the skin from erythema simultaneously during a long time adhesion is still a problem. The PPA is probably a solution for that. Since the soak of sweat always leads to erythema, permeability is vital in adhesive. We used PPA with different thicknesses to test the vapor permeability (Figure 3b). The result showed that when the thickness is less than 100 μm, the vapor permeability of PPA is good enough for daily work and sports. We tested the long-time adhesion property and biosafety of PPA by attaching it to the forearm for 48 h (Figure 3c). During the period, different sports were carried out for a total of 3 h (an hour each day) and an everyday shower was taken. The PPA could adhere firmly to the forearm with sweat, washing and other daily activities. And when peeling off the skin, the PPA could be mildly taken off without pain and residue. Previous research has shown that the PDMS and PEG oligomer is nontoxic and nonirritant to the skin. Hence, the biosafe material contributes to the excellent skin-compatible performance of PPA. The biosafety of PPA was compared with a commercial KINESIO patch and a nonpermeable copper foil. The comparison of close-up pictures for skin before and after 48 h covering was done in Figure 3c. The pictures indicated that the PPA showed the best biosafety with only red spots caused by the removal of fine hair, while the Kinesio patch and copper foil led to more red spots after the 48 h covering.

2.3. PPA-MPC Adhesive Strain Sensor for Motion Detection

We people are experiencing different movements all the time. Having an accurate detection and monitoring of these movements will have a great significance in adjusting our behavior and helping our muscles and joints keep in good condition. The PPA is with low modulus and high elongation at break, which means it can have a comfortable and conformal contact with skin even with large deformation, making it a potential substrate for strain sensors to monitor the motion of humans on skin. The knee joint is the most significant part of our skin that deforms during daily life. The fully extended knee skin has 300% strain compared to the fully shrunk condition. Due to the great stretchability of PPA and liquid metal, PPA-MPC adhesive strain-sensor shows great potential for the motion detection of the knee joint.

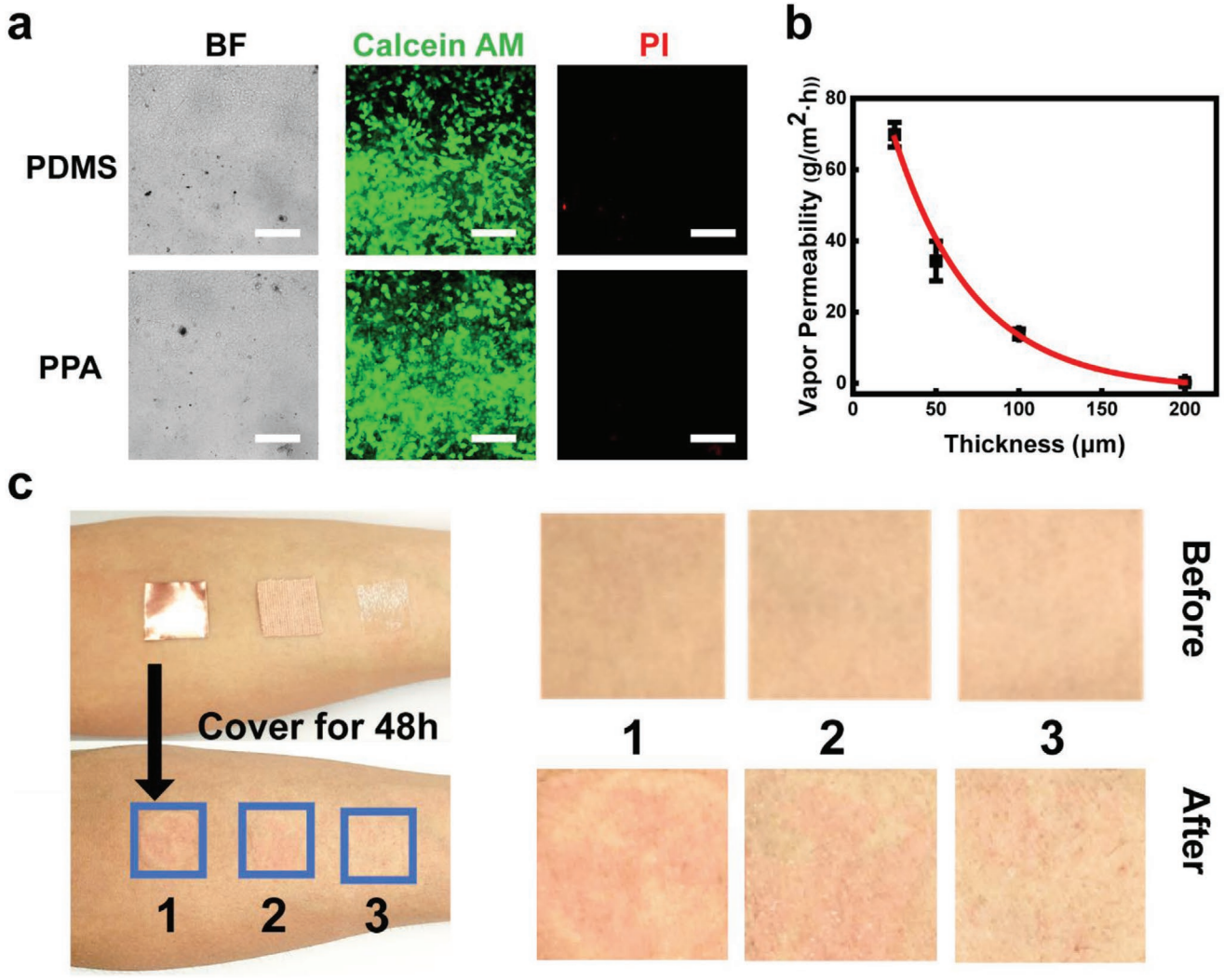

Figure 3. Cell viability, permeability, and skin-compatible performance of PPA. a) Cell viability of PDMS and PPA (scale bar: 200 μm). b) Permeability test of the PPA with different thicknesses. c) On skin biosafety test using the copper foil, the Kinesio, and the PPA.

The fabrication of PPA-MPC electronics is straightforward. We prepared the conductive ink by sonicating liquid metal in decanol and screen-printed the ink onto PET release paper. The precursor of PPA was spin-coated onto the circuits and cured after vacuum degassing. After the curing process, we used a peel-off method to finish the fabrication of PPA-MPC electronics and sintering the circuits at the same time. By increasing the time of vacuum degassing, the ratio of circuits transferred onto PPA can be increased as well (Figure S7, Supporting Information).

We tested the mechanical and electromechanical performance of the PPA-MPC electronics. For the stress-stain curve, the PPA-MPC electronics showed significantly lower modulus and much higher elongation than PDMS-MPC electronics (**Figure 4**a). The change of resistance under different strain was tested and the strain sensor showed great accuracy and linearity with strain of 20%, 40%, 60%, and 80% respectively (Figure 4b), indicating its great potential in continuous accurate sensing. The strain sensor was stretched to 50% for 1000 cycles to characterize its durability. Clearly, it could bear this continuous deformation and maintain a stable resistance during the whole process (Figure 4c), which means the strain sensor is capable of longtime motion monitoring. The retention efficiency of PPA-MPC adhesive strain sensor after sports and showers were tested. We attached the strain sensor to the wrist and tested the peeling force after 30 min of sports or 30 min of shower. We could see a significant decrease in peeling force right after the sports because the sweat on the interface reduced the contact area. But when a press was applied on the strain sensor before the peeling test, the adhesion force returned to a high level due to the squeezed sweat and recovered contact area. And when the sweat was evaporated after 20 min, the adhesion force for samples without pressing restored to original level (Figure S8a, Supporting Information). For the shower test, we got similar result for the changing of adhesion force (Figure S8b, Supporting Information). We attached the strain sensor to the elbow and knee skin and bent it with different speeds continually (Figure 4d,g). The self-adhesive strain sensor

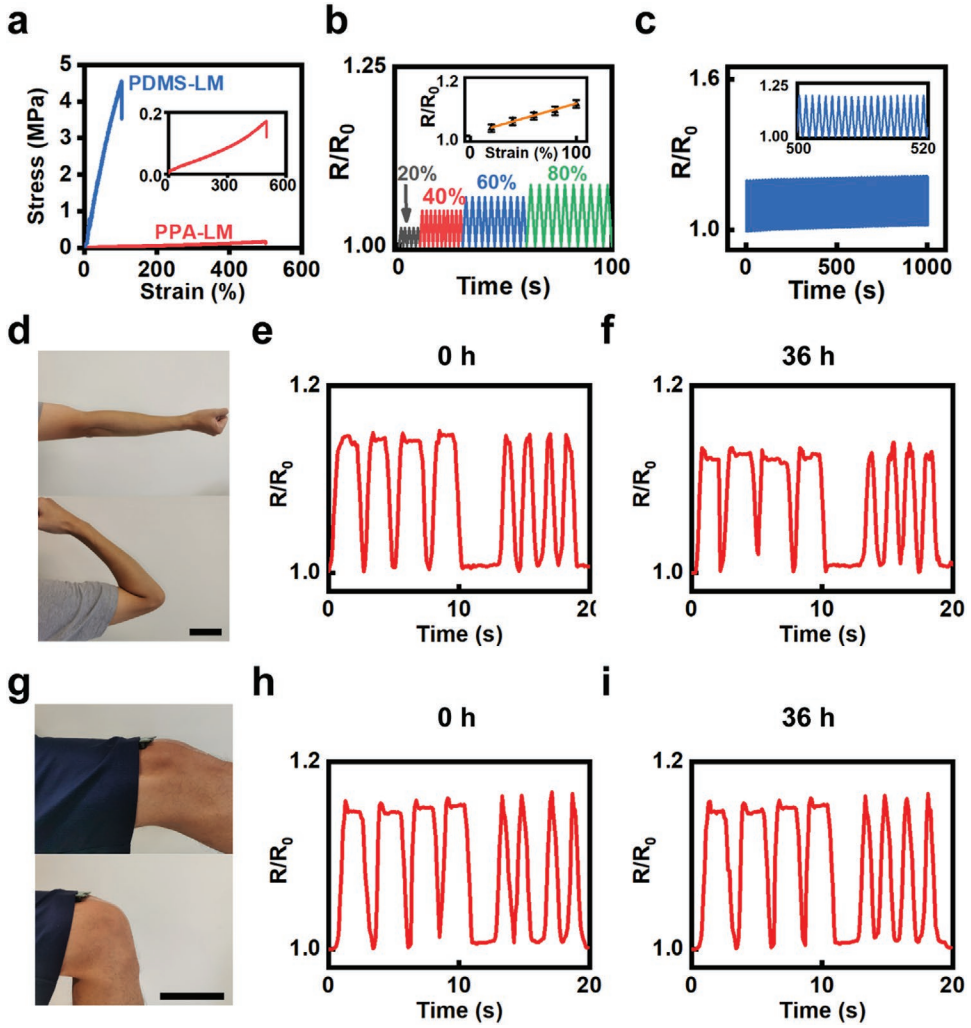

Figure 4. Performance of the PPA-MPC electronics and motion detection by PPA-MPC adhesive strain sensor. a) Stress–strain curve of PDMS-MPC electronics and PPA-MPC electronics. b) Change of resistance under different strain. c) Change of resistance during a 1000 cycle of 50% strain. d) Gestures for strain-sensor testing on the elbow (scale bar: 10 cm). e) Signals for strain-sensor testing on elbow before a 36 h wearing. f) Signals for strain-sensor testing on elbow after a 36 h wearing. g) Gestures for strain-sensor testing on the knee (scale bar: 10 cm). h) Signals for strain-sensor testing on the knee before a 36 h wearing. i) Signals for strain-sensor testing on the knee after a 36 h wearing.

could maintain stable adhesion and deform conformally with the skin. We carried out the same tasks after 36 h again. During this period, we did sports for an hour and take a shower for 30 min twice besides the daily work. The result showed that after a 36 h wearing, the strain sensor could still conformally adhere to the skin and showed the motion of the joint in real-time (Figure 4e,f,h,i).

2.4. PPA-MPC Adhesive Electrode for Electrophysiology

Nowadays, cardiovascular diseases, sports injury and degenerative diseases like Parkinson are prominent diseases that affect daily life.[52,53] Electrophysiology like electrocardiogram (ECG) and electromyogram (EMG) can show much information about the state of cardiovascular and muscle which means a lot in the prediction of the health problems.[54,55] The conformal contact between PPA-MPC and skin makes it a potential platform for electrophysiology detection of ECG and EMG. The fabrication process of the PPA-MPC adhesive electrode is similar to that of the self-adhesive strain-sensor; besides, the shape and size of the electrodes for ECG and EMG are the same of 20 mm^2. The round part is for better signal collection and the long lead helps decrease the contact with the nonsignal area which leads to less noise. The retention efficiency of PPA-MPC electrodes after sports and showers were tested using same method with PPA-MPC adhesive strain sensor. We could see the same trend for the changing of peeling force before and after sports, showers and different actions (Figure S8c,d, Supporting Information).

We attached the commercial electrodes and PPA-MPC adhesive electrodes near the wrist and recorded ECG signals by medical-grade ECG recorder (**Figure 5**a). We could see the P, QRS, and T waves were clear and distinguishable, with little noise and no baseline shift when attached first (Figure 5b,c). After 48 h of wearing, we recorded the ECG with the same operations. During this period, we did sports for an hour and

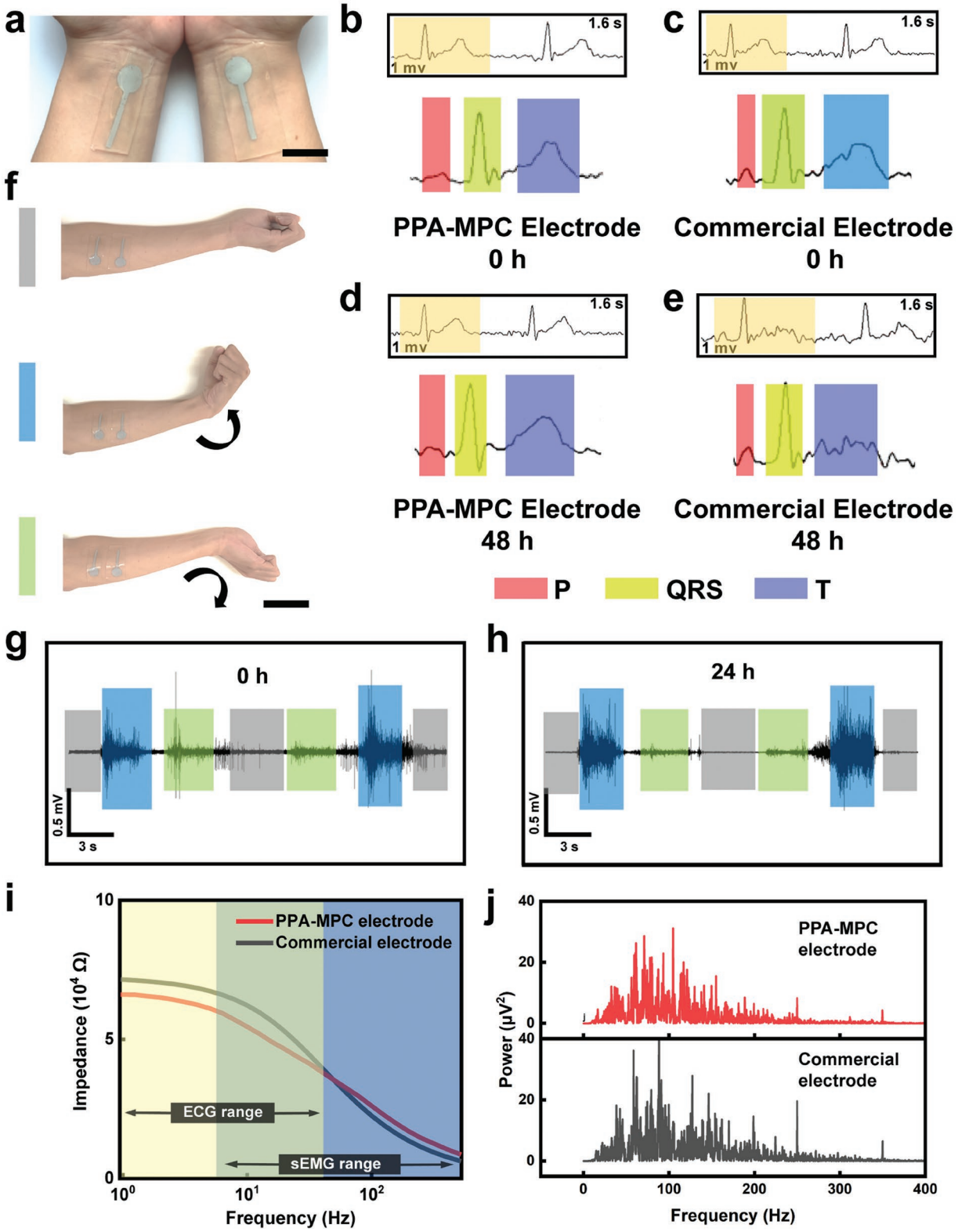

Figure 5. Performance of the commercial electrodes and PPA-MPC adhesive electrodes patch for electrophysiology. a) PPA-based self-adhesive electrodes patch for ECG detection (scale bar: 2 cm). b,c) ECG signal detected using PPA-MPC adhesive electrodes and commercial electrodes right after attaching. d,e) ECG signal detected using PPA-MPC adhesive electrodes and commercial electrodes after 48 h. f) Gestures for EMG signal testing (scale bar: 5 cm). g,h) EMG signal detected using PPA-MPC adhesive electrodes right after attaching and after 24 h. i) EIS of PPA-MPC adhesive electrodes and commercial electrodes. j) Power distribution at different frequencies of EMG signals detected using PPA-MPC adhesive electrodes and commercial electrodes.

took a shower for 30 min everyday besides the daily work. This time, the P, QRS, and T waves were still clear and distinguishable for the PPA-MPC adhesive electrodes without baseline shift, which indicated that the PPA-MPC adhesive electrodes could still maintain a robust and conformal contact with the specific forearm skin even with sweat and touches (Figure 5d). As for the commercial electrodes, due to the water loss of the hydrogel and the irreversible deformation of the rigid part after motion of the wrist, the baseline shift increased a lot after 48 h. (Figure 5e)

We attached two electrodes to the flexor carpi ulnaris as record electrodes and one on the bone of the wrist as the reference electrode to record the EMG signal of flexor carpi ulnaris using the PPA-MPC adhesive electrodes. We used three gestures to show different states of the muscle and detected the relative EMG signal, the upper one for the muscular contraction state, the medium one for the muscular extension state, and the lower one for the muscular relaxation state (Figure 5f). During the testing, we did the three in a specific order. The signal we collected was with significantly low noise of down to 5 μV which was barely seen in sEMG detection devices, and all the states of muscle activities could be distinguished for PPA-MPC adhesive electrodes right after attaching and after 24 h (Figure 5g,h). We carried out the same task using commercial electrodes for contrast and got a similar result (Figure S9, Supporting Information). The electrochemical impedance spectroscopy (EIS) of PPA-MPC adhesive electrodes and commercial electrodes were tested. At the low end of frequency, impedance for PPA-MPC electrodes was lower than that of the commercial electrodes; while at the high end of frequency, the opposite was true (Figure 5i). We analyzed the power distribution at different frequencies using different electrodes (Figure 5j). Clearly, the power distribution of signals collected from commercial electrodes and PPA-MPC adhesive electrodes were in agreement, indicating the effectiveness of the PPA-MPC adhesive electrodes in EMG signal detection.[56] The signal-noise ratios for the two electrodes were calculated and compared, and the PPA-MPC adhesive electrodes performed better because of a more conformally adhesion on the interface (Figure S10, Supporting Information).

2.5. PPA-MPC Adhesive Electrode for Wound Healing

Skin wound is one of the most common trauma appeared in the clinic. And how to accelerate the curing process is drawing extensive attention nowadays.[30,57] Pulsed electrical stimulation has been applied on skin wounds and showed great effect on advancing wound recovery, particularly in the phases of proliferation and remodeling.[58,59] We employed a skin wound model on rats and applied pulsed electrical stimulation through the self-adhesive electrodes.

A wound with a diameter of two centimeters was created on the back of each rat and the adhesive electrodes were attached to the skin around the wound and connected to an electrical stimulation therapeutic equipment (**Figure 6**a). The pictures of the wound in two groups were recorded on Day 0, Day 4, Day 7 and Day 10, respectively, and we could see the significant difference between the control group and the electrical stimulation (ES) group (Figure 6b). The wound area for ES group was much smaller than that of the control group after applied the treatment, and the wound closure time decreased a lot as well. Images of hematoxylin and eosin (H&E) stained wound tissues showed that the treated ones showed scar formed on day 4, fibroblast proliferation and vascular formed on day 7 and mature epidermis and hair follicles formed on day 10. While the untreated ones showed much slower healing process (Figure 6c). Images of Masson stained wound tissues showed that the ES group showed larger area and higher density of blue colored collagen fiber contents for each sample time than those in the control group, indicating a better wound healing effect (Figure 6d). The accelerated wound healing results demonstrated that the PPA based electrodes show great potential for personalized medical treatment.

3. Conclusion

In conclusion, we presented a facile method of providing an MPC made with PPA that encapsulated gallium-based liquid metal alloy circuits as epidermal electronics. The obtained electronics showed lower modulus (<50 kPa), higher elongation (>400%) and excellent biosafety than pristine PDMS. The electronics could conformally adhere to skin and meet the needs for stable monitoring of joint motion and electrophysiological signal after sports and showers. We used an animal model and proved the adhesive electronics could also be applied to significantly accelerate the skin wound healing process. We believe our work will be generally useful for material scientists, electrical engineers, biologists and doctors in creating more complex and advanced bioelectronics for accurate diagnosis and effective treatment.

4. Experimental Section

Materials and Instruments: PEG oligomer (Mw = 200400800), ethanol, and decanol were obtained from Alladin. PDMS base and curing agent (Sylgard 184) were obtained from Dow Corning. Eutectic gallium-indium (EGaIn) liquid metal was obtained from Beijing Hawk Technology Co., Ltd. Cell live/dead kit was obtained from Invitrogen, USA. Commercial foam 2228 monitoring electrodes were obtained from 3M, USA.

All sonications were carried out using a sonicator (Scientz, Scientz-IID). Mechanical tests and adhesion tests were carried out using a tensile track (Instron 3365, USA). SEM images were collected from Zeiss Merlin at an acceleration voltage of 5 kV. AFM images were collected from MFP-3D, Asylum Research, USA. Rheology test was performed using a rheometer (MARS III). The water contact angle was tested using the Drop Shape Analyzer (KRUSS). Cell fluorescence images were obtained by confocal microscopy (Zeiss LSM 710). The change of resistance was tested using an electrochemical workstation (1040C, CHI, China). The deformation during the electrochemical tests was applied by a guide rail (FSL 40, FUYU, China). Electrode-skin impedance measurement was tested with Multi Autolab/M204 potentiostat (Metrohm, Switzerland). Electromyogram (EMG) signals were collected using a g.HIamp multi-channel biosignal amplifier (G.tec, Austria).

Fabrication of the PPA: PDMS base and curing agent was added into a plastic cup by a ratio of 10:1, then the different amounts of PEG oligomer were added into the precursor by different weight ratio. The precursor was mixed well and degassed under vacuum for an hour

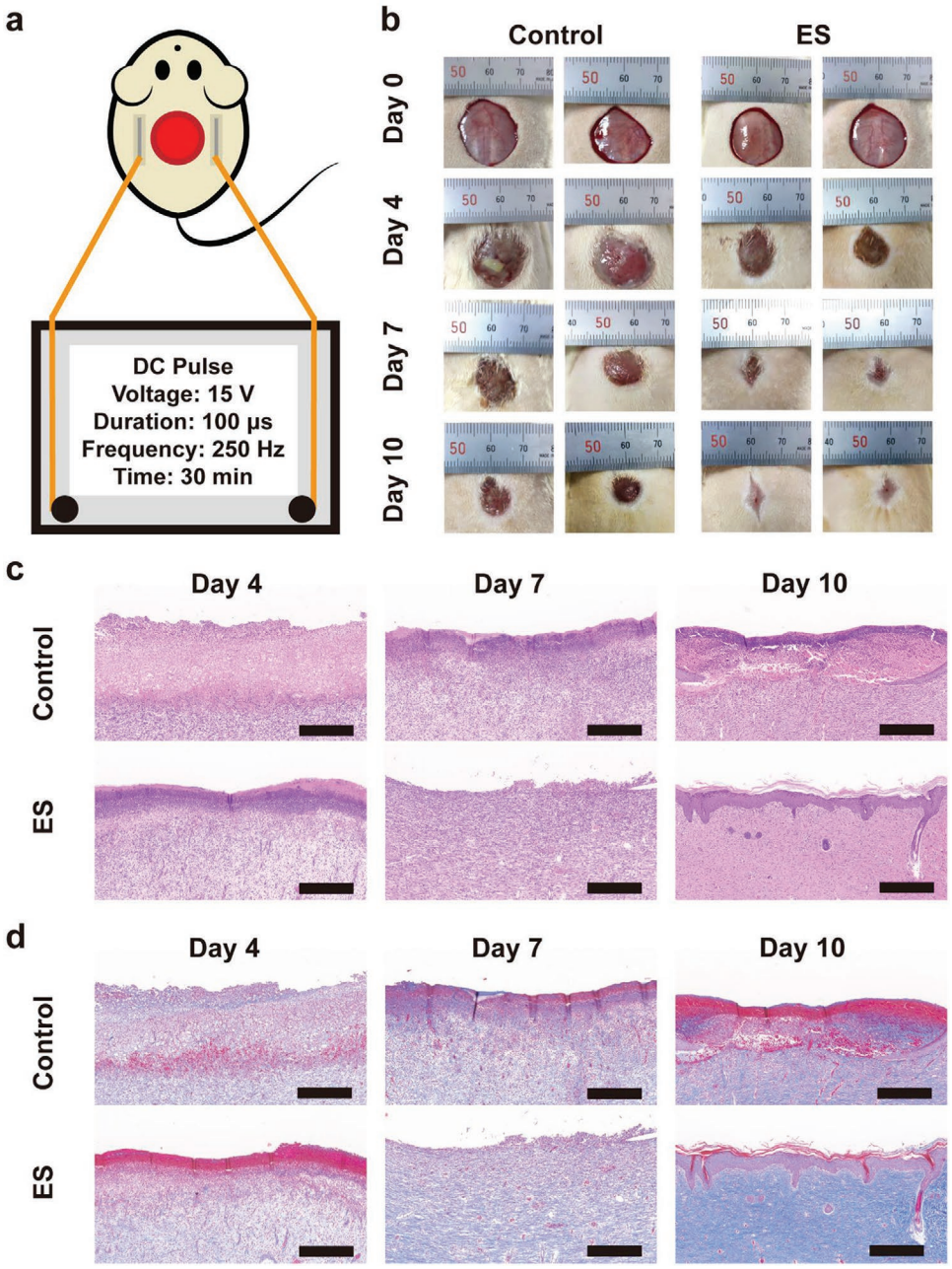

Figure 6. Wound healing model using PPA-MPC adhesive electrode. a) Experimental setup showing PPA-MPC adhesive electrodes near the skin wound on the back of mice and the electrical stimulation parameters for wound healing. b) Photos of the wound on day 0, day 4, day 7, and day 10. c) Images of hematoxylin-eosin stained wound tissues on day 4, day 7, and day 10. d) Images of Masson stained wound tissues on day 4, day 7, and day 10 (scale bar: 200 µm).

before spin-coated on a flat substrate. PPA was obtained by curing the mixer at 80 °C for an hour.

Fabrication of PPA-MPC Adhesive Epidermal Electronics: 2.5 g of EGaIn and 500 µL decanol were added into a 5 mL tube and sonicated for 1 min (strength: 18%) to obtain conductive ink for screen printing. The ink was screen-printed on the PET release paper and baked in an oven at 80 °C for 20 min to remove the residual solvent. Then, the well-mixed precursor of PPA was poured on the circuits, spin-coated for specific parameter, placed in vacuum chamber for an hour, and baked at 80 °C oven for an hour to obtain the PPA with the liquid metal circuits. Finally, a peel-off method was used to fully or partially transfer the liquid metal circuits onto the PPA and sinter the circuits at the same time.

Characterization of Mechanical and Adhesion Properties: The sample size for mechanical test was 15 mm wide, 50 mm long, and 300 µm thick and the stroke speed of the tensile test was 100 mm min^{-1}. The modulus of the PPA was calculated using the measured sectional area.

Before the adhesion testing, the forearm skin was cleaned with a mixed solution of deionized water and ethanol. The sample was cured on a plastic film and cut into 15 mm wide, 50 mm long, and 300 µm thick for the test. During the test, the stroke speed was kept at 15 mm s^{-1}. The nonelastic plastic film was kept during the test for eliminating the effect of deformation.

Swelling Test and Sol Extraction Test: The as-prepared PDMS and PPA were cut into square samples with side length of 15 mm and thickness of 300 µm and weighed. Then the samples were kept in a glass bottle with

cyclohexane for 7 d to reach fully swollen state and then weighed. The swelling ratio was calculated by dividing weight of swollen samples by weight of original samples.

The sol extraction test was similar to that of the swelling test, using cyclohexane as solvent. The fully swollen sample samples were dried for 3 d inside the fuming cupboard and weighed. The gel fraction was calculated by dividing weight of dried samples by weight of original samples.

Rheology Test and Water Contact Angle of PDMS and PPA: The PDMS and PPA samples were prepared and cut into appropriate size and placed on the rheometer. The frequency was selected from 0.1 to 100 Hz and the storage modulus and loss modulus of samples were collected using shear mode.

The PDMS and PPA samples were cured on a flat glass slide. Before the test, the instrument was adjusted to horizontal state and samples were cleaned by gas flow. Then the samples were placed on the instrument and the pictures and angles of different time were collected using the computer connected to the instrument.

Cell Viability, Permeability Test, and Skin-Compatible Performance of the PPA: The PPA film and PPA-MPC electronic were first immersed in fibronectin solution to promote the adhesion of cells. Human umbilical vein endothelial cells (HUVECs) were seeded on the surface and cultured in DMEM supplemented with 10% fetal bovine serum under 5% CO2 and 37 °C for 7 d. Live/dead kits were added in the dish for cell viability tests. The fluorescent images were taken by confocal microscopy.

The permeability test was carried out using a PPA film and a plastic dish. The weights of the 35 mm plastic dishes were measured using a scale. Then 10 g of ultrapure water was added to every dish and the dishes were placed to a bigger dish to avoid the influence of airflow on the evaporation of water. Finally, the PPA films with different thicknesses were weighed using a scale and then covered on the surface of dishes and set for 48 h. The weight of PPA film and water in the dish were tested every 12 h.

The skin-compatible performance of the PPA was evaluated on the human forearm skin. One volunteer participated in this study. Three samples (thin PPA film, thick KINESIO tape and nonpermeable copper foil) were attached to the skin of the forearms of the volunteer and worn for 48 h. The skin was photographed before and after the test so that the appearance could be compared.

Electromechanical Performance and Electrochemical Impedance Spectroscopy of PPA-MPC Electronics: Electromechanical performance of PPA-MPC adhesive electrode was tested with a guide rail and an electrochemical workstation. For testing the influence of velocity, the distance was 50% strain of the sample and the velocity was changed. For the durable test, the velocity was fixed at 40 mm s^{-1} and the distance was 50% strain of the sample. The electrochemical workstation was set to *i–t* curve at a potential of 0.05 V and the sampling rate was 20 Hz.

Electrode-skin impedance measurement of PPA-MPC adhesive electrode was tested with a potentiostat. The frequency range was selected to be from 10 Hz to 1 kHz. Two working PPA-MPC adhesive electrodes were adhered on the flexor carpi ulnaris (FCU) muscle, and reference electrode was adhered on the elbow. Commercial electrodes were used for comparison with a same process. The surface contact area for both electrodes is 200 mm^2.

Joint Motion and Electrophysiological Detection Using the Adhesive Epidermal Electronics: The PPA-MPC adhesive electrode was adhered to the knee and elbow joint, and different tasks were carried out that caused the deformation of the skin near the joints, leading to the change of resistance of the circuits, which could be detected using an electrochemical workstation.

The PPA-MPC adhesive electrode was adhered to the wrist skin and the electrodes were connected to a commercialized medical-grade ECG recorder to collect electrocardiogram (ECG) signals. For surface electromyography (sEMG), two working electrodes were adhered on the FCU muscle and ground electrode was adhered to the wrist bone. The electrodes were connected to a multichannel amplifier for bipolar sEMG signal collection with a sampling frequency of 1200 Hz and an analog notch filter at 48–52 Hz. The SNR for both electrodes were calculated using the equation below

$$\mathrm{SNR}\,(dB) = 10\log_{10}\left(\frac{P_{\mathrm{signal}}}{P_{\mathrm{noise}}}\right) = 20\log_{10}\left(\frac{A_{\mathrm{signal}}}{A_{\mathrm{noise}}}\right) \quad (1)$$

The P_{signal} refers to the power of signal, the P_{noise} refers to the power of noise, the A_{signal} refers to the amplitude of signal, and the A_{noise} refers to the amplitude of noise.

All on-human tests were carried out on the skin of authors and approved by the Medical Ethics Committee of Southern University of Science and Technology (No. 2021SYG049). Signed informed consent has been obtained from the volunteers involved in the experiments.

Wound Healing Model Using the Adhesive Epidermal Electronics: First, rats were divided into two groups and anesthetized with isoflurane. Dorsal hair was removed with an electric clipper and hair removal cream. A wound with a diameter of 2 cm was cut and the PPA-MPC adhesive electrodes was adhered to the skin near the wound and connected to an electrical stimulation therapeutic equipment. The pulsed electrical stimulation was applied to the rats for 30 min d^{-1} during the experiment. Images shown were all taken from the same mouse. Samples of the wound were harvested on day 4, day 7, and day 10. H&E stain and Masson stain were utilized for the histology. All animal protocols were approved by the Institutional Animal Care and Use Committee at Southern University of Science and Technology (No. SUSTech-JY202108022).

Supporting Information

Supporting Information is available from the Wiley Online Library or from the author.

Acknowledgements

The authors thank Shenzhen Science and Technology Program (KQTD20190929172743294), the National Natural Science Foundation of China (21535001, 81730051, 32071390, 12072082, and 12125202), the National Key R&D Program of China (2018YFA0902600), the Chinese Academy of Sciences (QYZDJ-SSW-SLH039 and 121D11KYSB20170026), Shenzhen Bay Laboratory (SZBL2019062801004), Shenzhen Key Laboratory of Smart Healthcare Engineering (ZDSYS20200811144003009), Guangdong Innovative and Entrepreneurial Research Team Program (2019ZT08Y191), GBA Research Innovation Institute for Nanotechnology (2020GN0110), and Tencent Foundation through the XPLORER PRIZE for financial support. The authors acknowledge the assistance of SUSTech Core Research Facilities. The authors are grateful to Dr. Ruihua Dong for the help of animal experiment, Miss Le Wang for the WCA test, Mr. Zeyang Pang for the rheology test, and Mr. Li Ding for the SEM image.

Conflict of Interest

The authors declare no conflict of interest.

Author Contributions

J.C. and X.J. conceived the idea. J.C. designed and completed most of the experiments and data analysis. J.S. helped with the fabrication of liquid metal circuits and tests of the strain sensor. S.Y. took the AFM image and helped with detection and analysis of the EMG signal. J.D. did the cell viability test, helped with the fabrication of PPA-MPC, and helped with the test of skin-compatibility. X.J. and X.S. supervised the project, interpreted the results, and revised the paper. All the authors took part in the discussion and writing.

Data Availability Statement

The data that support the findings of this study are available from the corresponding author upon reasonable request.

Keywords

adhesives, bioelectronics, health monitoring, liquid metals, treatment

Received: January 12, 2022
Revised: March 4, 2022
Published online:

[1] J. Kim, P. Gutruf, A. M. Chiarelli, S. Y. Heo, K. Cho, Z. Xie, A. Banks, S. Han, K.-I. Jang, J. W. Lee, K.-T. Lee, X. Feng, Y. Huang, M. Fabiani, G. Gratton, U. Paik, J. A. Rogers, *Adv. Funct. Mater.* **2017**, *27*, 1604373.
[2] J. Kim, A. Banks, Z. Xie, S. Y. Heo, P. Gutruf, J. W. Lee, S. Xu, K.-I. Jang, F. Liu, G. Brown, J. Choi, J. H. Kim, X. Feng, Y. Huang, U. Paik, J. A. Rogers, *Adv. Funct. Mater.* **2015**, *25*, 4761.
[3] G. H. Lee, H. Moon, H. Kim, G. H. Lee, W. Kwon, S. Yoo, D. Myung, S. H. Yun, Z. Bao, S. K. Hahn, *Nat. Rev. Mater.* **2020**, *5*, 149.
[4] X. Yu, Z. Xie, Y. Yu, J. Lee, A. Vazquez-Guardado, H. Luan, J. Ruban, X. Ning, A. Akhtar, D. Li, B. Ji, Y. Liu, R. Sun, J. Cao, Q. Huo, Y. Zhong, C. Lee, S. Kim, P. Gutruf, C. Zhang, Y. Xue, Q. Guo, A. Chempakasseril, P. Tian, W. Lu, J. Jeong, Y. Yu, J. Cornman, C. Tan, B. Kim, et al., *Nature* **2019**, *575*, 473.
[5] S. Wang, J. Xu, W. Wang, G. J. N. Wang, R. Rastak, F. Molina-Lopez, J. W. Chung, S. Niu, V. R. Feig, J. Lopez, T. Lei, S. K. Kwon, Y. Kim, A. M. Foudeh, A. Ehrlich, A. Gasperini, Y. Yun, B. Murmann, J. B.-H. Tok, Z. Bao, *Nature* **2018**, *555*, 83.
[6] R. Dong, Y. Liu, L. Mou, J. Deng, X. Jiang, *Adv. Mater.* **2019**, *31*,1805033.
[7] W. Gao, H. Ota, D. Kiriya, K. Takei, A. Javey, *Acc. Chem. Res.* **2019**, *52*, 523.
[8] B. C.-K. Tee, A. Chortos, R. R. Dunn, G. Schwartz, E. Eason, Z. Bao, *Adv. Funct. Mater.* **2014**, *24*, 5427.
[9] J. R. Sempionatto, M. Lin, L. Yin, E. De la paz, K. Pei, T. Sonsa-ard, A. N. de Loyola Silva, A. A. Khorshed, F. Zhang, N. Tostado, S. Xu, J. Wang, *Nat. Biomed. Eng.* **2021**, *5*, 737.
[10] C. Wang, X. Li, H. Hu, L. Zhang, Z. Huang, M. Lin, Z. Zhang, Z. Yin, B. Huang, H. Gong, S. Bhaskaran, Y. Gu, M. Makihata, Y. Guo, Y. Lei, Y. Chen, C. Wang, Y. Li, T. Zhang, Z. Chen, A. P. Pisano, L. Zhang, Q. Zhou, S. Xu, *Nat. Biomed. Eng.* **2018**, *2*, 687.
[11] E. Song, J. Li, S. M. Won, W. Bai, J. A. Rogers, *Nat. Mater.* **2020**, *19*, 590.
[12] Y. S. Choi, Y. Y. Hsueh, J. Koo, Q. S. Yang, R. Avila, B. W. Hu, Z. Q. Xie, G. Lee, Z. Ning, C. Liu, Y. M. Xu, Y. J. Lee, W. K. Zhao, J. Fang, Y. J. Deng, S. M. Lee, A. Vazquez-Guardado, I. Stepien, Y. Yan, J. W. Song, C. Haney, Y. S. Oh, W. T. Liu, H. J. Yoon, A. Banks, M. R. MacEwan, G. A. Ameer, W. Z. Ray, Y. G. Huang, T. Xie, et al., *Nat. Commun.* **2020**, *11*, 5990.
[13] Y. Liu, J. Li, S. Song, J. Kang, Y. Tsao, S. Chen, V. Mottini, K. McConnell, W. Xu, Y.-Q. Zheng, J. B.-H. Tok, P. M. George, Z. Bao, *Nat. Biotechnol.* **2020**, *38*, 1031.
[14] L. Tang, J. Shang, X. Jiang, *Sci. Adv.* **2021**, *7*, eabe3778.
[15] R. Dong, L. Wang, C. Hang, Z. Chen, X. Liu, L. Zhong, J. Qi, Y. Huang, S. Liu, L. Wang, Y. Lu, X. Jiang, *Small* **2021**, *17*, 2006612.
[16] S. Cheng, C. Hang, L. Ding, L. Jia, L. Tang, L. Mou, J. Qi, R. Dong, W. Zheng, Y. Zhang, X. Jiang, *Matter* **2020**, *3*, 1664.
[17] L. Ding, C. Hang, S. Cheng, L. Jia, L. Mou, L. Tang, C. Zhang, Y. Xie, W. Zheng, Y. Zhang, X. Jiang, *ACS Nano* **2020**, *14*, 16770.
[18] C. Hang, L. Ding, S. Cheng, R. Dong, J. Qi, X. Liu, Q. Liu, Y. Zhang, X. Jiang, *Adv. Mater.* **2021**, *33*, 2101447.
[19] M. Mahmood, S. Kwon, H. Kim, Y.-S. Kim, P. Siriaraya, J. Choi, B. Otkhmezuri, K. Kang, K. J. Yu, Y. C. Jang, C. S. Ang, W.-H. Yeo, *Adv. Sci.* **2021**, *8*, 2101129.
[20] P. Makvandi, R. Jamaledin, G. J. Chen, Z. Baghbantaraghdari, E. N. Zare, C. Di Natale, V. Onesto, R. Vecchione, J. Lee, F. R. Tay, P. Netti, V. Mattoli, A. Jaklenec, Z. Gu, R. Langer, *Mater. Today* **2021**, *47*, 206.
[21] H. Lee, B. P. Lee, P. B. Messersmith, *Nature* **2007**, *448*, 338.
[22] S. Baik, D. W. Kim, Y. Park, T.-J. Lee, S. Ho Bhang, C. Pang, *Nature* **2017**, *546*, 396.
[23] C. Zhang, B. Wu, Y. Zhou, F. Zhou, W. Liu, Z. Wang, *Chem. Soc. Rev.* **2020**, *49*, 3605.
[24] C. Zhang, Y. Zhou, H. Han, H. Zheng, W. Xu, Z. Wang, *ACS Nano* **2021**, *15*, 1785.
[25] H. Jung, M. K. Kim, J. Y. Lee, S. W. Choi, J. Kim, *Adv. Funct. Mater.* **2020**, *30*, 2004407.
[26] S. Li, L. Wang, W. Zheng, G. Yang, X. Jiang, *Adv. Funct. Mater.* **2020**, *30*, 2002370.
[27] S. Ji, C. Wan, T. Wang, Q. Li, G. Chen, J. Wang, Z. Liu, H. Yang, X. Liu, X. Chen, *Adv. Mater.* **2020**, *32*, 2001496.
[28] L. Zhang, K. S. Kumar, H. He, C. J. Cai, X. He, H. Gao, S. Yue, C. Li, R. C.-S. Seet, H. Ren, J. Ouyang, *Nat. Commun.* **2020**, *11*, 4683.
[29] L. Mou, Y. Xia, X. Jiang, *Anal. Chem.* **2021**, *93*, 11525.
[30] G. L. Grove, C. R. Zerweck, B. P. Ekholm, G. E. Smith, N. I. Koski, *J. Wound Ostomy Continence Nurs.* **2014**, *41*, 40.
[31] K. Jang, S. Y. Han, S. Xu, K. E. Mathewson, Y. Zhang, J. Jeong, G. Kim, R. C. Webb, J. W. Lee, T. J. Dawidczyk, R. H. Kim, Y. M. Song, W. Yeo, S. Kim, H. Cheng, S. Il Rhee, J. Chung, B. Kim, H. U. Chung, D. Lee, Y. Yang, M. Cho, J. G. Gaspar, R. Carbonari, M. Fabiani, G. Gratton, Y. Huang, J. A. Rogers, *Nat. Commun.* **2014**, *5*, 4779.
[32] J. Huang, Y. Cai, C. Xue, J. Ge, H. Zhao, S. H. Yu, *Nano Res.* **2021**, *14*, 3636.
[33] S. H. Jeong, S. Zhang, K. Hjort, J. Hilborn, Z. Wu, *Adv. Mater.* **2016**, *28*, 5830.
[34] D. Cho, R. Li, H. Jeong, S. Li, C. Wu, A. Tzavelis, S. Yoo, S. S. Kwak, Y. Huang, J. A. Rogers, *Adv. Mater.* **2021**, *33*, 2103857.
[35] J. H. Kim, S. R. Kim, H. J. Kil, Y. C. Kim, J. W. Park, *Nano Lett.* **2018**, *18*, 4531.
[36] Z. Gu, X. Wan, Z. Lou, F. Zhang, L. Shi, S. Li, B. Dai, G. Shen, S. Wang, *ACS Appl. Mater. Interfaces* **2019**, *11*, 1496.
[37] Y. Tan, X. Dai, Y. Li, D. Zhu, *J. Mater. Chem.* **2003**, *13*, 1069.
[38] M. D. Dickey, *Adv. Mater.* **2017**, *29*, 1606425.
[39] T. Daeneke, K. Khoshmanesh, N. Mahmood, I. A. de Castro, D. Esrafilzadeh, S. J. Barrow, M. D. Dickey, K. Kalantar-zadeh, *Chem. Soc. Rev.* **2018**, *47*, 4073.
[40] H. Wang, Y. Yao, Z. He, W. Rao, L. Hu, S. Chen, J. Lin, J. Gao, P. Zhang, X. Sun, X. Wang, Y. Cui, Q. Wang, S. Dong, G. Chen, J. Liu, *Adv. Mater.* **2019**, *31*, 1901337.
[41] Q. Zhuang, Z. Ma, Y. Gao, Y. Zhang, S. Wang, X. Lu, H. Hu, C. Cheung, Q. Huang, Z. Zheng, *Adv. Funct. Mater.* **2021**, *31*, 2105587.
[42] Y. Lu, Q. Hu, Y. Lin, D. B. Pacardo, C. Wang, W. Sun, F. S. Ligler, M. D. Dickey, Z. Gu, *Nat. Commun.* **2015**, *6*, 10066.
[43] Y. Ren, X. Sun, J. Liu, *Micromachines* **2020**, *11*, 200.
[44] R. Guo, X. L. Wang, W. Z. Yu, J. B. Tang, J. Liu, *Sci. China Technol. Sci.* **2018**, *61*, 1031.
[45] L. Tang, L. Mou, J. Shang, J. Dou, W. Zhang, X. Jiang, *Mater. Horiz.* **2020**, *7*, 1186.
[46] X. Wang, Y. Zhang, R. Guo, H. Wang, B. Yuan, J. Liu, *J. Micromech. Microeng.* **2018**, *28*, 034003.
[47] X. Wang, L. Fan, J. Zhang, X. Sun, H. Chang, B. Yuan, R. Guo, M. Duan, J. Liu, X. Wang, L. Fan, B. Yuan, R. Guo, M. Duan, J. Liu, J. Zhang, X. Sun, H. Chang, *Adv. Funct. Mater.* **2019**, *29*, 1907063.
[48] X. Wang, Y. Ren, J. Liu, *Micromachines* **2018**, *9*, 360.
[49] R. W. Style, R. Boltyanskiy, B. Allen, K. E. Jensen, H. P. Foote, J. S. Wettlaufer, E. R. Dufresne, *Nat. Phys.* **2015**, *11*, 82.

[50] S. Zeng, R. Li, S. G. Freire, V. M. M. Garbellotto, E. Y. Huang, A. T. Smith, C. Hu, W. R. T. Tait, Z. Bian, G. Zheng, D. Zhang, L. Sun, *Adv. Mater.* **2017**, *29*, 1700828.
[51] C. Dagdeviren, Y. Shi, P. Joe, R. Ghaffari, G. Balooch, K. Usgaonkar, O. Gur, P. L. Tran, J. R. Crosby, M. Meyer, Y. Su, R. Chad Webb, A. S. Tedesco, M. J. Slepian, Y. Huang, J. A. Rogers, *Nat. Mater.* **2015**, *14*, 728.
[52] J. A. A. G. Damen, L. Hooft, K. G. M. Moons, *Lancet* **2018**, *391*, 1867.
[53] B. R. Bloem, M. S. Okun, C. Klein, *Lancet* **2021**, *397*, 2284.
[54] J. Valls-Solé, F. Valldeoriola, E. Tolosa, M. J. Marti, *Brain* **1997**, *120*, 1877.
[55] Y. Fang, Y. Zou, J. Xu, G. Chen, Y. Zhou, W. Deng, X. Zhao, M. Roustaei, T. K. Hsiai, J. Chen, *Adv. Mater.* **2021**, *33*, 2104178.
[56] R. Merletti, S. Muceli, *J. Electromyogr. Kinesiol.* **2019**, *49*, 102363.
[57] G. Torkaman, *Adv. Wound Care* **2014**, *3*, 202.
[58] H. Kai, T. Yamauchi, Y. Ogawa, A. Tsubota, T. Magome, T. Miyake, K. Yamasaki, M. Nishizawa, *Adv. Healthcare Mater.* **2017**, *6*, 1700465.
[59] F. Ershad, A. Thukral, J. Yue, P. Comeaux, Y. Lu, H. Shim, K. Sim, N. I. Kim, Z. Rao, R. Guevara, L. Contreras, F. Pan, Y. Zhang, Y. S. Guan, P. Yang, X. Wang, P. Wang, X. Wu, C. Yu, *Nat. Commun.* **2020**, *11*, 3823.